

Article

Explicit Identification of Pointwise Terrain Gradients for Speed Compensation of Four Driving Tracks in Passively Articulated Tracked Mobile Robot

Haneul Jeon  and Donghun Lee 

Mechanical Engineering Department, Soongsil University, Seoul 06978, Republic of Korea

* Correspondence: dhlee04@ssu.ac.kr

Abstract: Tracked mobile robots can overcome the limitations of wheeled and legged robots in environments, such as construction and mining, but there are still significant challenges to be addressed in terms of trajectory tracking. This study proposes a kinematic strategy to improve the trajectory-tracking performance of a PASTRo (Passively Articulated Suspension based Track-typed mobile robot), which comprises four tracks, two rockers, a differential gear, and a main body. Due to the difficulties in explicitly identifying track-terrain contact angles, suspension kinematics is used to identify track-terrain contact angles (TTCA) in arbitrarily rough terrains. Thus, the TTCA-based driving velocity projection method is proposed in this study to improve the maneuverability of PASTRo in arbitrarily rough terrains. The RecurDyn-Simulink co-simulator is used to examine the improvement of PASTRo compared to a tracked mobile robot non-suspension version. The results indicate that PASTRo has a 33.3% lower RMS (Root Mean Square) distance error, 56.3% lower RMS directional error, and 43.2% lower RMS offset error than the four-track skid-steer mobile robot (SSMR), even with planar SSMR kinematics. To improve the maneuverability of PASTRo without any information on the rough terrain, the TTCA is calculated from the suspension kinematics, and the TTCA obtained is used for both TTCA-based driving velocity projection methods. The results show that PASTRo, with the TTCA-based driving velocity projection method, has a 39.2% lower RMS distance error, 57.9% lower RMS directional error, and 51.9% lower RMS offset error than the four-track SSMR.

Keywords: skid-steer mobile robot; terrain gradient; velocity propagation; track typed mobile robot; passively articulated suspension

MSC: 70B15

Citation: Jeon, H.; Lee, D. Explicit Identification of Pointwise Terrain Gradients for Speed Compensation of Four Driving Tracks in Passively Articulated Tracked Mobile Robot. *Mathematics* **2023**, *11*, 905. <https://doi.org/10.3390/math11040905>

Academic Editors: Paolo Mercorelli, Oleg Sergiyenko and Oleksandr Tsybmal

Received: 11 January 2023
Revised: 7 February 2023
Accepted: 8 February 2023
Published: 10 February 2023



Copyright: © 2023 by the authors. Licensee MDPI, Basel, Switzerland. This article is an open access article distributed under the terms and conditions of the Creative Commons Attribution (CC BY) license (<https://creativecommons.org/licenses/by/4.0/>).

1. Introduction

For several decades, there have been many studies on MRs in rough terrains in aerospace [1,2], industry [3,4], and military [5–8] applications. A disaster rescue robot [9] has consistently been developed for a mission at the scene of accidents, and the DARPA robotics challenge was held to motivate the development of disaster robots that could do “complex tasks in dangerous, degraded, human-engineered environments” instead of humans [10,11].

The MRs driving on rough, rugged, and uneven terrains can be classified into wheel, leg, and track-typed MRs in terms of their locomotion mechanisms. Over the past decade, numerous research projects on legged robots have been carried out. Especially the two famous quadrupedal robots, Spot of the Boston Dynamics [6] and Cheetah of MIT, started showing remarkable results in their quadrupedal locomotion. Additionally, the most noteworthy characteristic of such quadrupedal MRs would be the possibility of various gait pattern generation.

However, despite such advantages of quadrupedal locomotion, wheel and track-driven MRs are still being studied because securing posture stability in steering control of

quadrupedal locomotion is evaluated to be somewhat more complicated than the wheel and track-driven MRs. The Mars rover Curiosity, composed of six wheels with rocker-bogie suspension, has already shown remarkable results in NASA's Mars missions [2]. The Packbot of the iRobot [7] for reconnaissance missions is composed of two tracks for driving, and two tilting tracks for both driving and overcoming obstacles. In particular, several MRs with passively or actively articulated suspensions for driving stabilities on rough terrains have been presented [12,13]. The rocker-bogie suspension used in the Mars rovers, and the Shrimp suspension proposed by Siegwart [12] is the most popular passively articulated suspension structures.

In the case of the rocker-bogie system, it is possible to reduce the motion of the main body when surmounting sizable obstacles by pitching the motion of a rocker and bogie mounted on each side of the rover. However, there are no rolling joints in the rockers, bogies, and wheels to passively and independently adapt their orientations to the ground surfaces inclined in the transverse direction. Then, the lack of rolling joints may lead to loss of traction between the wheel and ground at specific postures due to improper contact. According to simulation results performed in our laboratory, it is confirmed that the inappropriate contact of a driving wheel with the ground may lead to peak torques in the other driving wheels and poor driving performances during the entire driving. In designing MR for driving on such unknown terrains, it is natural for a designer to think of the peak torque and the torque distribution as one of the most critical factors in selecting the driving motors. Therefore, in an aspect of the mechanical design, the effect of the passive rolling joints in the suspensions, or driving modules should be considered for improving driving performances on rough terrains. Especially as the four tracks are supposed to passively maximize the contact area between operating modules and the grounds.

In control of the skid-steer MR, the linear and angular velocities of MR are typically expressed in an inertial coordinate frame under the assumption of the coplanar contact of all driving wheels or tracks with grounds. Under this assumption, Caracciolo, Luca et al. [14]; Kozłowski, Krzysztof, and Dariusz Pazderski [15]; and Shuang, Gao et al. [16] calculated the velocity control input of a skid-steering MRs by solving kinematics in XY-plane of the inertial coordinate. However, the motion of MRs on rough terrains should be described in three-dimensional space due to geometric complexities of the ground. Especially in cases of the MRs with passively articulated suspensions for connecting the main body and four driving tracks, each driving track may have arbitrary orientations relative to the main body. That is, it is evident that the MR kinematics should not be enough for precise posture tracking control due to no consideration of the tilting angle of the driving track.

In previous research, Tarokh, Mahmoud et al. [17] proposed a kinematic model for the Mars rover that can estimate the wheel-terrain contact angle of driving modules by considering the 6-DOF motion of the rocker-bogie suspension. However, the research only focused on reducing the effects of slippage for given elevation maps by compensating for differences between wheel-terrain contact points. Thus, in case of insufficient information on the elevation map of the ground, such an elevation map-dependent method should not be used to expect satisfactory trajectory tracking performances in unknown terrains.

Thus, a new MR mechanism named PASTRo (passively articulated suspension-based track-typed MR), which was previously published [18,19] by this author, is composed of four tiltable driving tracks, two rockers, a main body, and a differential gear module connecting two rockers are proposed. Moreover, the main contributions of this study include the following:

1. The suspension kinematics-based speed compensation methods are newly proposed to successfully calculate the track-terrain contact angles (TTCA) at any arbitrary rough terrains without a pointwise terrain elevation map.
2. Then, the uncertainties in the kinematic parameters of MR kinematics and the relative orientation of the driving track can be successfully removed.

3. The proposed algorithm is evaluated through simulation and experimental results, demonstrating improved trajectory tracking performance compared to traditional control methods.
4. Additionally, the paper includes an analysis of the robustness and stability of the proposed algorithm under different operating conditions.
5. Overall, this research aims to contribute to the advancement of tracked mobile robot technology and its potential applications in various fields.

This paper is organized as follows: Section 2 describes the design of a track-typed MR composed of four tracks, and passively articulated suspensions similar to the rocker. Section 3 describes MR kinematics for posture tracking control of MR on rough terrains. Primarily, the suspension kinematics to estimate the inclination of driving tracks on arbitrary rough terrains is described. Then, a way to compensate for the gradient effect by considering the inclination of driving tracks obtained by the suspension kinematics is described. In Section 4, the locomotive simulation to verify improvements in posture tracking performances by applying the proposed gradient effect compensator is conducted in a virtual environment in RecurDyn-Simulink co-simulator. Additionally, the results of posture tracking performances impro

2. A New Quad-Tracked Mobile Robot with Passively Articulated Suspensions

This section describes all details regarding the new track-typed mobile mechanism with passively articulated suspension for improving its mobility in rough terrains. The proposed MR comprises the main body, four passively tiltable driving tracks, two rockers, a differential gear, and passive pitch-roll joints between the rocker and the driving track. The differential gear enables relative pitching of the left and right suspensions and induces the same pitching on the left and right with respect to the chassis, resulting in the chassis' posture stability and the track's ground contact smoothly. By passive motions dependent on the contact geometry of the rough terrains, the pose of each driving track can be properly and independently determined to maximize the contact areas between driving modules and the grounds, as shown in Figure 1. Thus, this MR can always secure the proper contact with the ground in all driving tracks without any additional control efforts.

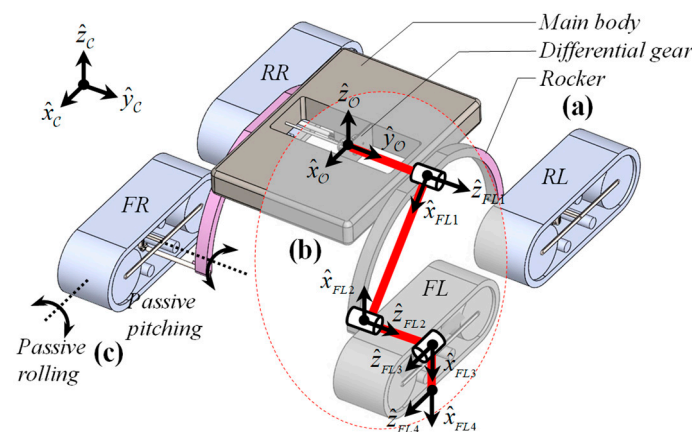


Figure 1. Proposed quad-tracked MR: (a) four driving tracks connected with main body with rocker, (b) joint coordinate frames assigned to the front left suspension as an example of suspension kinematics, (c) 2-dof pitch-roll joints for passively connecting rockers and driving tracks.

As shown in Figure 1, the instantaneous center of rotation (ICR) frame and the center of mass (COM) frame are denoted as $\mathcal{C} - xyz$ and $\mathcal{O} - xyz$ in this paper, respectively. The 2-dof passive joint between rocker and track is assembled in the order of pitch and roll to maintain z axes of the driving tracks to be parallel with heading axis of the main body on any arbitrary rough terrains. For securing orientation stabilities of all driving tracks at any arbitrary contact terrains, the intersecting points of pitch and roll axes should be

located at middle of the tracks in transverse direction and slightly lower down from center of the tracks in height direction. Each passive joint has intentional $\pm 20^\circ$ joint limits, which prevents the decline of orientation stability of MR due to excessive tilting on steep slope. When the difference of height between left and right side on terrain is significantly large, differential-gear make the main body retain stability by having average pitch angle between left and right rocker.

3. MR Kinematics for Rough Terrains

This section describes the overall posture tracking control strategy of the proposed MR on arbitrary rough terrains as shown in Figure 2. In Section 3.1, the planar kinematics of the skid-steer mobile robot (SSMR) is described first to calculate the required track angular speeds for the desired linear velocity and angular velocity of the MR. Section 3.2 describes the suspension kinematics to calculate the driving tracks' poses relative to the main body on arbitrary rough terrains. Then, gradient effect compensator (GEC) for considering the unavoidably varying driving tracks' attitudes will be detailed in Section 3.3. In updating the driving speed consecutively calculated from planar SSMR kinematics and the GEC, a critical violation of the assumption about driving speeds obtained from the SSMR kinematics inevitably occurred. The violation may lead to slippage in the contact area due to differences in front and rear driving velocities on the same side. Additionally, the front or rear track can be tilted up and unintentionally lose contact with the ground due to the differences in driving speed. Thus, at the end of Section 3.3, the backward velocity propagation of the updated front driving velocity to the rear driving track is proposed to prevent the undesired track pitching phenomena.

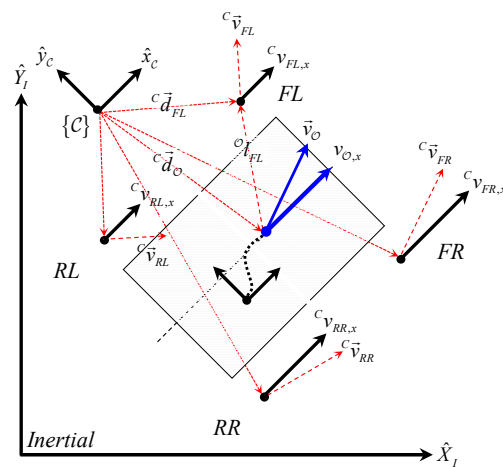


Figure 2. Coordinate frames of conventional planar SSMR kinematics defined on the inertial XY-plane. The z axes of the frame {C} and {O} are all out of the page.

3.1. Planar SSMR Kinematics

As shown in Figure 2, in the planar SSMR kinematics, the frame {O} and frame {pq} located at the center of mass (COM) of MR and the driving tracks, respectively are expressed in the XY-plane of the frame {C} located at the instantaneous center of rotation. Here, $p \in \{F, R\}$, $q \in \{L, R\}$, FR (front right), FL (front left), RR (rear right), and RL (rear left) are indices for defining the suspension kinematics and driving track positions, respectively. The linear and angular velocities of the frame {O} is also expressed in the frame {C}, as shown in Figure 2.

For given desired linear and angular velocities of the main body in its steering motions, the driving track speeds can be calculated using following Equations (1) and (2):

$$\frac{\|v_{pq,x}\|}{\|c_{d_{pq,y}}\|} = \frac{\|v_{O,x}\|}{\|c_{d_{O,y}}\|} = |\omega_O| \tag{1}$$

where,

$${}^C \vec{d}_O = [x_O, y_O, 0]^T \tag{2}$$

where, ${}^C \vec{d}_O$ denotes position of origin of the frame $\{O\}$ relative to the frame $\{C\}$. For given linear velocity of the main body in x -direction and angular velocity of the main body, the radius of instantaneous center of rotation, y_O , can be calculated with following Equation (3):

$$y_O = \frac{v_{O,x}}{\omega_O} \tag{3}$$

For given input ${}^C v_{O,x}$ and ${}^C \omega_{O,z}$ expressed in frame $\{C\}$, the linear track speeds can be calculated as follows:

$$\begin{bmatrix} {}^C v_{pL,x} \\ {}^C v_{pR,x} \end{bmatrix} = \begin{bmatrix} 1 & -l_{pL,y} \\ 1 & l_{pR,y} \end{bmatrix} \cdot \begin{bmatrix} {}^C v_{O,x} \\ {}^C \omega_{O,z} \end{bmatrix} \tag{4}$$

From Equations (1)–(4), the following equality constraint between the front and rear driving speeds on the same side can be obtained with the assumption of identical driving speed on the same side. ${}^C v_{pL,x}$ and ${}^C v_{pR,x}$ denote the linear speeds of the left and right driving tracks, respectively.

$$\begin{cases} {}^C v_{pL,x} = {}^C v_{FL,x} = {}^C v_{RL,x} \\ {}^C v_{pR,x} = {}^C v_{FR,x} = {}^C v_{RR,x} \end{cases} \tag{5}$$

3.2. Suspension Kinematics

As shown in Figure 1, the frame $\{O\}$ is chosen as a common reference frame for four cases of the suspension kinematics. Table 1 represents the screw axes expressed in the frame $\{O\}$ for the suspension kinematics at its zero position. The zero position means that all joint values set equal to zero. The $l_1, l_2, l_3,$ and l_4 parameters are the constant link parameters of the suspension structure.

Table 1. Screw axes $({}^O S_{(pq,i)} = (\omega_i, v_{(pq,i)}))$ expressed in the frame $\{O\}$ for the suspension kinematics from main body.

i	ω_i	$v_{FL,i}$	$v_{FR,i}$	$v_{RR,i}$	$v_{RL,i}$
1	(0, 1, 0)	(0, l_1 , 0)	(0, $-l_1$, 0)	(0, $-l_1$, 0)	(0, l_1 , 0)
2	(0, 1, 0)	($l_2 \cdot c\theta_s, l_1, -l_2 \cdot s\theta_s$)	($l_2 \cdot c\theta_s, -l_1, -l_2 \cdot s\theta_s$)	($-l_2 \cdot c\theta_s, -l_1, -l_2 \cdot s\theta_s$)	($-l_2 \cdot c\theta_s, l_1, -l_2 \cdot s\theta_s$)
3	(1, 0, 0)	($l_2 \cdot c\theta_s, l_1 + l_3, -l_2 \cdot s\theta_s$)	($l_2 \cdot c\theta_s, -l_1 - l_3, -l_2 \cdot s\theta_s$)	($-l_2 \cdot c\theta_s, -l_1 - l_3, -l_2 \cdot s\theta_s$)	($-l_2 \cdot c\theta_s, l_1 + l_3, -l_2 \cdot s\theta_s$)
4	(1, 0, 0)	($l_2 \cdot c\theta_s, l_1 + l_3, -l_2 \cdot s\theta_s - l_4$)	($l_2 \cdot c\theta_s, -l_1 - l_3, -l_2 \cdot s\theta_s - l_4$)	($-l_2 \cdot c\theta_s, -l_1 - l_3, -l_2 \cdot s\theta_s - l_4$)	($-l_2 \cdot c\theta_s, l_1 + l_3, -l_2 \cdot s\theta_s - l_4$)

Equation (6) represents the product of exponentials (PoE) formula describing the suspension kinematics from $\{O\}$ to $\{pq4\}$. All screw axes in Equation (6) are expressed in the frame $\{O\}$ as Table 1.

$${}^O_{pq4} T = e^{[S_{pq,1}]\theta_1} e^{[S_{pq,2}]\theta_2} e^{[S_{pq,3}]\theta_3} e^{[S_{pq,4}]\theta_4} {}^O_{pq4} M = \begin{bmatrix} {}^O_{pq4} R & {}^O_{pq4} \vec{l} \\ 0_{1 \times 3} & 1 \end{bmatrix} \tag{6}$$

where θ_1 denotes angular displacement of differential gear that connects right and left side rockers. θ_2 and θ_3 denote pitch and roll of the driving tracks, respectively. θ_4 is set to zero, because the transformation from $\{pq3\}$ to $\{pq4\}$ is pure translation. The positive rotation about these axes is by the usual right-hand rule. $e^{[S]\theta}$ represents the matrix exponential of the $[S]\theta \in se(3)$. The $[S] \in \mathbb{R}^{4 \times 4}$ denotes 4×4 matrix representation of unit screw

axis $\mathcal{S} \in \mathbb{R}^6$, and θ is the joint angle. ${}^{\mathcal{O}}_{pq4}M$ denotes the configuration of the frame $\{pq4\}$ relative to the frame $\{\mathcal{O}\}$ when the suspension is in its zero position. The relative position ${}^{\mathcal{O}}\vec{l}_{pq4} \in \mathbb{R}^3$ and orientation ${}^{\mathcal{O}}_{pq4}R \in SO(3)$ of the frame $\{pq4\}$ relative to the frame $\{\mathcal{O}\}$ can be obtained from the following suspension kinematics.

As shown in Equation (7), the obtained ${}^{\mathcal{O}}\vec{l}_{pq4}$ and ${}^{\mathcal{O}}_{pq4}R$ are used to calculate the driving speed ${}^{\mathcal{O}}v_{pq4,x} \in \mathbb{R}$ with considering the relative pose between the main body and the pq driving track.

$${}^c v_{pq,x} = {}^c S_X \cdot \left\{ {}^c \vec{\omega}_{\mathcal{O}} \times \left({}^c \vec{d}_{\mathcal{O}} + {}^{\mathcal{O}}R \cdot \left({}^{\mathcal{O}}\vec{l}_{pq4} \right) \right) \right\} = v_{\mathcal{O},x} - \omega_{\mathcal{O},z} (l'_{pq4,y}) \tag{7}$$

The driving speed vector ${}^c \vec{v}_{pq}$ can be calculated by the cross product of ${}^c \vec{\omega}_{\mathcal{O}}$ and ${}^c \vec{d}_{pq4}$. The selection vector ${}^c S_X$ is then applied, so as to extract the heading component of the driving velocity ${}^c v_{pq,x}$. By applying Equation (6) to FL, RL, RR , and FR driving tracks, an explicit relationship between the track speed ${}^c v_{track}$ and the MR velocity ${}^c \mathbf{V}$ can be clarified as follows:

$${}^c \mathbf{v}_{track} = {}^c \begin{bmatrix} v_{FL,x} \\ v_{RL,x} \\ v_{RR,x} \\ v_{FR,x} \end{bmatrix} = \begin{bmatrix} 1 & -l'_{FL4,y} \\ 1 & -l'_{RL4,y} \\ 1 & -l'_{RR4,y} \\ 1 & -l'_{FR4,y} \end{bmatrix} \begin{bmatrix} {}^c v_{\mathcal{O},x} \\ {}^c \omega_{\mathcal{O},z} \end{bmatrix} = \Psi {}^c \mathbf{V} \tag{8}$$

Compensator input

$$\text{where, } l'_{pq4,y} = [0 \ 1 \ 0] \cdot {}^{\mathcal{O}}R \cdot {}^{\mathcal{O}}\vec{l}_{pq4}$$

where, the matrix Ψ denotes a Jacobian matrix for mapping linear and angular velocity of the frame $\{\mathcal{O}\}$ to the desired driving speeds. The reason why the distance vector $l'_{pq4,y}$ is included in Equations (6) and (8) is the distance from origin of the frame $\{\mathcal{O}\}$ to origin of the $pq4$ frame vary with passive rolling motion of driving track relative to the rockers as shown in Figure 3.

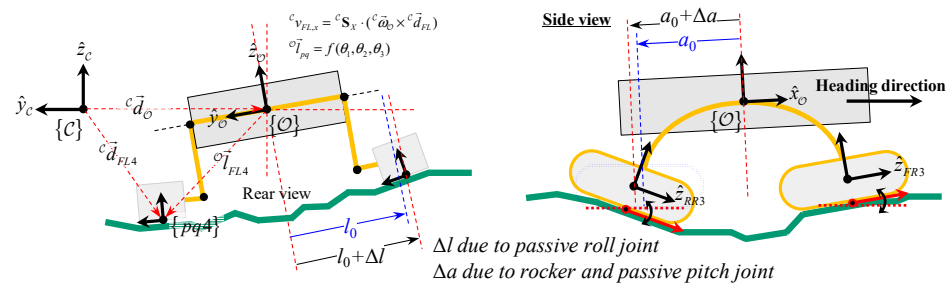


Figure 3. Variation of the transverse distances between the main body and driving track due to passive rolling motion of the driving track.

3.3. GEC Based Terrain Gradient Identification and Backward Velocity Propagation

The driving tracks are mechanically assembled with the main body through the passively articulated suspension. Thus, it is clear that the track driving speeds calculated from the planar SSMR kinematics cannot guarantee good posture tracking the performance of the MR at any arbitrary rough terrains, as shown in Figure 3, since the ICR changes according to the change in the relative pose of the driving track with respect to the main chassis. This can be referred to as the gradient effect (GE), inevitably caused by variations of the track-terrain contact angle (TTCA) in the rough terrain control.

3.3.1. Driving Speed Compensation

Figure 4 shows the overall GEC framework including feedback information from the suspension kinematics and MR. While the ${}^C\mathbf{v}_{track} \in \mathbb{R}^4$ obtained from Equation (8) is a track speed to achieve the ${}^Cv_{O,x}$ and ${}^C\omega_{O,z}$, it does not still include the relative orientation between the driving track and XY-plane of the frame $\{C\}$.

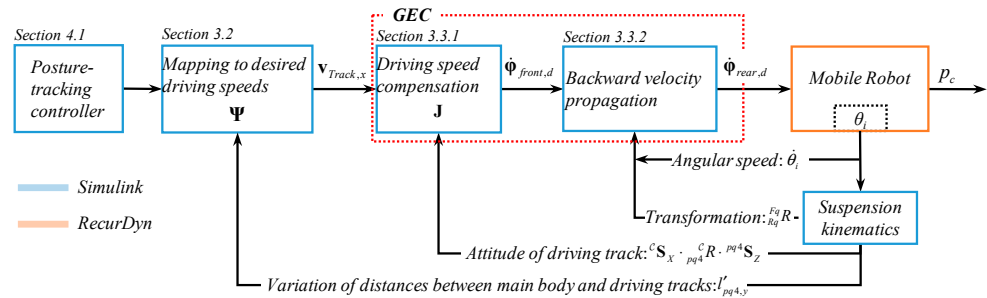


Figure 4. Detailed block diagram of the posture tracking control strategy of the proposed MR including the GEC with backward velocity propagation and feedbacks from the suspension kinematics.

For each driving track, the track angular speed $\dot{\phi}_{pq}$ for the desired ${}^Cv_{pq,x}$ can be calculated through following Equation (9) considering the track-terrain contact angle (TTCA) relative to the frame $\{C\}$.

$${}^C\mathbf{S}_x \cdot ({}^C_{pq4}R^{pq4} [0 \ 0 \ r\dot{\phi}_{pq}]^T) = {}^Cv_{pq,x} \tag{9}$$

Obtained from Eq.(6)

where, r denotes an effective track radius and ${}^C_{pq4}R$ denotes orientation of the driving track relative to the frame $\{C\}$. Equation (9) can be rearranged to the following form:

$$\dot{\phi}_{pq} = \left(r^{-1} \cdot \frac{1}{{}^C\mathbf{S}_x \cdot {}^C_{pq4}R \cdot pq4\mathbf{S}_z} \right) \cdot {}^Cv_{pq4,x} \tag{10}$$

The term ${}^C\mathbf{S}_x \cdot {}^C_{pq4}R$ denotes a direction cosine of the relative orientation of frame $\{pq4\}$ with respect to the frame $\{C\}$ as shown in Figure 3. Then, by integrating Equations (8) and (10), a GE-compensated track angular speed $\dot{\phi}_{pq}$ can be directly calculated from the ${}^C\mathbf{V}$ As follows:

$$\dot{\phi}_{pq} = (rK)^{-1} [1 \ -l'_{pq4,y}] \begin{bmatrix} {}^Cv_{O,x} \\ {}^C\omega_{O,z} \end{bmatrix} \tag{11}$$

where, $K = {}^C\mathbf{S}_x \cdot {}^C_{pq4}R \cdot pq4\mathbf{S}_z$

As a result, by applying Equation (11) to all driving tracks, the resultant relationship between the desired track angular speed vector $\dot{\phi}$ and the MR velocity ${}^C\mathbf{V}$ can be packaged as follow Equation (12).

$$\dot{\phi} = \begin{bmatrix} \dot{\phi}_{FL} \\ \dot{\phi}_{RL} \\ \dot{\phi}_{RR} \\ \dot{\phi}_{FR} \end{bmatrix} = \begin{bmatrix} a_{FL} & -a_{FL}l'_{FL4,y} \\ a_{RL} & -a_{RL}l'_{RL4,y} \\ a_{RR} & -a_{RR}l'_{RR4,y} \\ a_{FR} & -a_{FR}l'_{FR4,y} \end{bmatrix} \cdot \begin{bmatrix} {}^Cv_{O,x} \\ {}^C\omega_{O,z} \end{bmatrix} = J{}^C\mathbf{V} \tag{12}$$

where, $\begin{cases} a_{pq} = (rK)^{-1} \\ {}^C_{pq4}R = {}^C_{R_O}{}^O R_{pq4} \in \mathbb{R}^{3 \times 3} \end{cases}$

Here, J denotes a Jacobian matrix for mapping the MR velocity expressed in frame $\{C\}$ to the desired track angular speed vector.

3.3.2. Backward Velocity Propagation for Preventing Undesired Track Pitching

According to Equation (12), it is confirmed that the speeds of four driving tracks can be independently calculated for given MR velocity with respect to the frame $\{C\}$. That is, when the postures of the driving track relative to the frame $\{C\}$ are obtained from the suspension kinematics, the loss of driving speed due to the differences in attitude between the XY -plane of the frame $\{C\}$, which is the reference frame of the planar SSMR kinematics, and the z -axis of the frame $\{pq4\}$ of the driving tracks can be successfully compensated. However, if the front and rear driving track on the same side are in different attitudes each other, the driving speeds obtained from Equation (11) will violate the SSMR kinematic assumptions in Equation (4). Additionally, this violation eventually leads to slippage in the ground due to differences in front and rear driving speeds on the same side. Then, either front or rear track can be unintentionally lifted up and lost their tractions between tracks and ground due to the inherent structural characteristics of the proposed MR.

An Intuitive way to resolve this issue inherently occurred in the passively tiltable structure is to impose new rear driving speeds dependent to the GEC-based front driving speeds, while maintaining to impose the GEC-based driving speeds to the front driving tracks and keep the holonomic constraints between the driving tracks and grounds. To calculate the rear driving speed generated by the front driving speed, we now choose the velocity propagation method in backward direction. A schematic diagram is detailed with a virtual single rigid link connecting two joints located in origins of the $\{Fq3\}$ and $\{Rq3\}$ in Figure 5. For given linear velocity of origin of the frame $\{Fq3\}$ and angular velocity of the link connecting $\{Fq3\}$ and $\{Rq3\}$, the linear velocity of origin of the frame $\{Rq3\}$ expressed in the frame $\{Rq3\}$ itself can be calculated by the backward velocity propagation in Equations (13)–(16). The linear velocity ${}^{Fq3}v_{Fq3}$ represents the front driving velocity obtained by the GEC. However, because it is impossible to directly calculate the angular velocity of the virtual link connecting $\{Fq3\}$ and $\{Rq3\}$ in Figure 5, a suspension based kinematic model from $\{Fq3\}$ to $\{Rq3\}$ should be developed for the actual backward velocity propagation. The coordinate frame assignment of the kinematic model is well detailed at Figure 5.

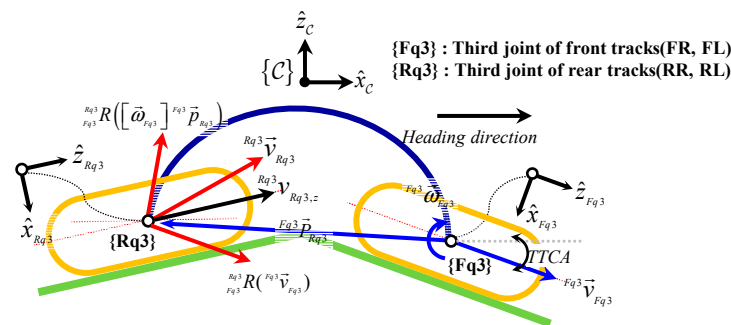


Figure 5. Schematic diagram of backward velocity propagation for calculating the rear driving speed in terms of the front driving speed.

To calculate the linear velocity of origin of the frame $\{Rq3\}$ expressed in the frame $\{Rq3\}$, we will now use Equation (13), starting from the frame $\{Fq3\}$, which is a based frame in this backward velocity propagation process, and has its linear velocity obtained from Equations (9)–(11). The linear velocity of the origin of frame $\{i + 1\}$ is the same as that of the origin of frame $\{i\}$, plus additional velocity component caused by the angular velocity of the link connecting joint $\{i\}$ and $\{i + 1\}$ as follows:

$${}^i\vec{v}_{i+1} = {}^i\vec{v}_i + \vec{\omega}_i \times {}^i\vec{p}_{i+1} = {}^i\vec{v}_i + [\vec{\omega}_i] {}^i\vec{p}_{i+1} \tag{13}$$

Here, ${}^i\vec{v}_{i+1}$ and ${}^i\vec{v}_i$ denotes the linear velocity of the origin of frame $\{i + 1\}$ and $\{i\}$ with respect to the frame $\{i\}$, respectively. ${}^iP_{i+1}$ is the position of the origin of frame

$\{i + 1\}$ and $\{i\}$ with respect to the frame $\{i\}$. The matrix $[\vec{\omega}_i]$ is a 3×3 skew-symmetric matrix representation of the angular velocity vector ω_i of the link expressed in frame $\{i\}$. Then, the linear velocity of the origin of frame $\{Rq3\}$ relative to the frame $\{Fq3\}$ can be calculated as follows:

$${}^{Fq3}\vec{v}_{Rq3} = {}^{Fq3}\vec{v}_{Fq3} + [\vec{\omega}_{Fq3}]{}^{Fq3}\vec{p}_{Rq3} \tag{14}$$

As mentioned earlier, because it is impossible to directly calculate the angular velocity of the link connecting $\{Fq3\}$ and $\{Rq3\}$ in Figure 5, a following formula using $SO(3)$ transformation from $\{Fq3\}$ to $\{Rq3\}$ is used to calculate the angular velocity. Then, the angular velocity can be calculated by multiplying a time derivative of the $SO(3)$ matrix by its transpose as follows:

$$[\vec{\omega}_{Fq3}] = \begin{bmatrix} 0 & -\omega_{Fq3,z} & \omega_{Fq3,y} \\ \omega_{Fq3,z} & 0 & -\omega_{Fq3,x} \\ -\omega_{Fq3,y} & \omega_{Fq3,x} & 0 \end{bmatrix} = {}^{Fq3}\dot{R}_{Rq3} {}^{Fq3}R_{Rq3}^T \tag{15}$$

After multiplying both sides of Equation (14) by ${}^{Fq3}R^T$, the track angular speed can be obtained by the inner product of ${}^{Rq3}v_{Rq3}$ and ${}^{Rq3}S_Z = [0 \ 0 \ 1]^T$ as follows:

$$\dot{\varphi}_{Rq3} = r_{track}^{-1} \left\{ S_{Rq3,z} \cdot {}^{Fq3}R_{Rq3}^T \left({}^{Fq3}\vec{v}_{Fq3} + [\vec{\omega}_{Fq3}]{}^{Fq3}\vec{p}_{Rq3} \right) \right\} \tag{16}$$

4. Verification of the Single GEC and Backward Velocity Propagation Combined GEC

4.1. Posture Tracking Controller

The reference velocity q_r and error posture p_e expressed in the ICR frame are selected as control inputs for the posture tracking controller, as shown in Figure 6. Since the position and the orientation of the MR can be measured with respect to the inertial frame using GPS and AHRS sensors, the following coordinate transformation should be conducted as shown in Equation (17):

$${}^C p_e = {}^C \begin{bmatrix} x_e \\ y_e \\ \theta_e \end{bmatrix} = {}^C_I R \cdot {}^I(p_r - p_c) = {}^C_I R \cdot {}^I \begin{bmatrix} x_r - x_c \\ y_r - y_c \\ \theta_r - \theta_c \end{bmatrix} \tag{17}$$

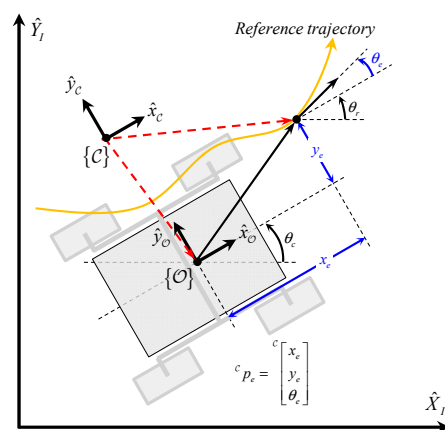


Figure 6. Posture error for the posture tracking controller.

The control algorithm shown in Equation (18) for posture tracking control is applied in this study as follows: The stability of the proposed posture tracking controller is based on the Lyapunov stability theorem, which provides a mathematical proof of the stability of the system. The stability of the proposed controller was already evaluated through both

simulation and experimental results [20], which showed that the controller was able to maintain stability in a variety of operating conditions.

$${}^C \mathbf{V} = \begin{bmatrix} {}^C v_{O,x} \\ {}^C \omega_{O,x} \end{bmatrix} = C \begin{bmatrix} v_r \cos \theta_r + K_x x_e \\ \omega_r + v_r (K_y y_e + K_\theta \sin \theta_e) \end{bmatrix} \quad (18)$$

where K_x , K_y , and K_θ are positive constants, position error gains, and orientation error gains, respectively. The design of the controller gains was based on extensive testing and tuning, with the goal of finding the optimal balance between stability and performance.

4.2. Simulation

As shown in Figure 7, the performances of posture tracking control of the PASTRo with the proposed gradient effect compensator are verified in the RecurDyn-Simulink co-simulator. In this research, the maneuverability is chosen as the performance index for the posture-tracking control on rough terrain. All mechanical parameters of the PASTRo in the RecurDyn simulator are represented in Table 2.

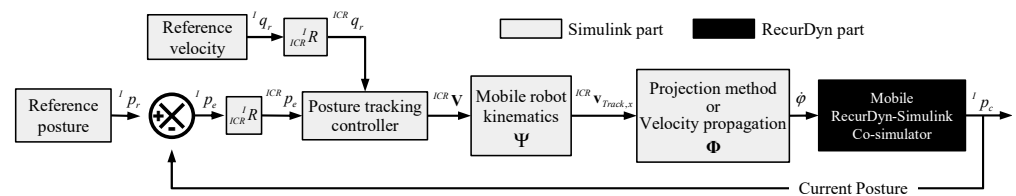


Figure 7. Overall simulation framework to verify the performance of the (1) TTCA-based driving velocity projection method and (2) velocity propagation driving velocity projection method based on the RecurDyn-Simulink co-simulator.

Table 2. Mechanical dimensions of 3D model of PASTRo for proposed simulation.

	Symbol	Unit	Value
Total mass		kg	1400.7
Main body mass		kg	512.8
Track mass		kg	470
Center of Mass	COM, x		0.03
	COM, y	mm	−0.12
	COM, z		−236.80
Total height	H1	mm	612
Total width	W1	mm	1670
Total length	L	mm	1760
Wheelbase	W2	mm	1377
Track diameter	D	mm	267.6
Track height	H2	mm	314.5
Track width	W3	mm	291
Roll joint height	H3	mm	90

The terrain and reference trajectory in these simulations are shown in Figure 8. The amplitude of the sinusoidal-shaped terrain is set to 629 mm, four times the driving track’s height, and two times the total height of PASTRo, as shown in Table 3. The reference velocity remains constant at 1 m/s, the reference trajectory is set to a straight line, and its heading direction is set to an axis rotated 20 degrees about the z-axis of the inertial frame from the x-axis of the inertial frame, as shown in Figure 8. That is, the MR will traverse the sinusoidal terrain in diagonal with zero initial posture errors.

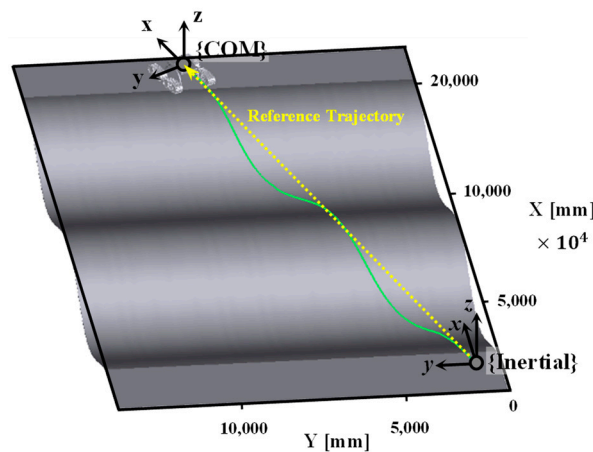


Figure 8. Reference trajectory and coordinate frames in the RecurDyn simulation model.

Table 3. Parameters of rough terrain and posture tracking controller for simulation.

Terrain	Total length	22,000 mm
	Total width	14,000 mm
	Amplitude	629 mm
	Period	8800 mm
Reference (in inertial frame)	Velocity	1000 mm/s
	Trajectory	Straight Line
Initial Posture (in inertial frame)	Position	Origin (0,0)
	Orientation	$\theta = 0$
Simulation	Sampling time	1 ms (Total 22 s)
	Step	22,000
Posture error gain	K_x	1
	K_y	10^{-6}
	K_θ	10^{-3}
Track Friction Coefficient	Dynamic	1
	Static	1.4

4.3. Performance Indices

Table 4 shows three conventional performance indices for the terrainability, maneuverability, and trafficability proposed by D. Apostopoulos [21], and these have been widely used to evaluate the performance of MRs.

Table 4. Previous works for evaluation of mobile robot mechanisms.

Author	Performance Index	Analysis Model	Driving Terrain
Takafumi Haji et al. [22]	Maneuverability	Dynamics model in 3D space	Flat ground
Michaud, S., & Richter, L [23]	Terrainability Trafficability	Dynamics model in 3D space	Stairs and blocks
Zhang, Peng et al. [24]	Terrainability Trafficability	Dynamics model in 3D space	blocks
Ding, Liang et al. [25]	Terrainability Maneuverability Trafficability	Dynamics model in 3D space	Rough terrains

Table 4. Cont.

Author	Performance Index	Analysis Model	Driving Terrain
Thuer, T., and Siegwart, R [26]	Terrainability	Dynamics model in 3D space	Stairs and blocks
Deng, Zongquan et al. [27]	Trafficability	Statics and kinematics model in 2D plane	Stairs and blocks
Gupta, A. K., & Gupta, V. K [28]	Terrainability Maneuverability	Dynamics model in 3D space	Stairs and slope
Nathaniel Steven Michaluk [29]	ESLV CESLV	Dynamics model in 2D plane	Blocks and slope
Paez, L., and Melo, K [30]	Terrainability, Maneuverability, Trafficability and Efficiency	Statics and kinematics model in 2D plane	Flat ground

These previous studies have shown that maneuverability is the most appropriate index to evaluate the posture-tracking performance of MRs. Haji [23] proposed maneuverability, distance, and heading angle error measures between the reference and actual trajectory in the XY-plane, and the two Haji indices and a position error in the y-direction were chosen as the performance indices in this study. The Haji indices are renamed as a distance error and a direction error, and the position error in the y-direction can be considered an offset distance error from the reference trajectory. The performance indices are described in the following Figure 9.

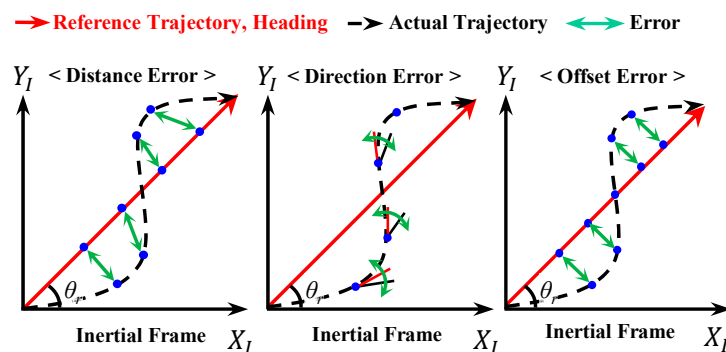


Figure 9. Definitions of the distance, direction and offset error for the maneuverability evaluation.

4.4. Simulation Results

For the comparison in this study, all parameters in the posture tracking control are equal. The distance, direction, and offset errors of a non-suspension version of the four-track SSMR and PASTRo are examined to verify the usefulness of the articulated suspension, as shown in Figure 10 and Table 5. While both the four-track SSMR and PASTRo show oscillatory behavior in all errors due to the terrain’s sinusoidal geometries, all errors in PASTRo are confirmed to be much smaller than those of the non-suspension version of a four-track SSMR. The root-mean-square (RMS) values of the distance, direction, and offset errors and their percentage differences are presented in Table 5 for comparison.

Table 5. Maneuverability performance value.

Performance Index	4-Track SSMR	4-Track SSMR with Suspension	
RMS distance error [mm]	130.8	87.2	43.6 [33.3%]
RMS direction error [Deg]	4.8	2.1	2.7 [56.3%]
RMS offset error [mm]	111.3	63.2	48.1 [43.2%]

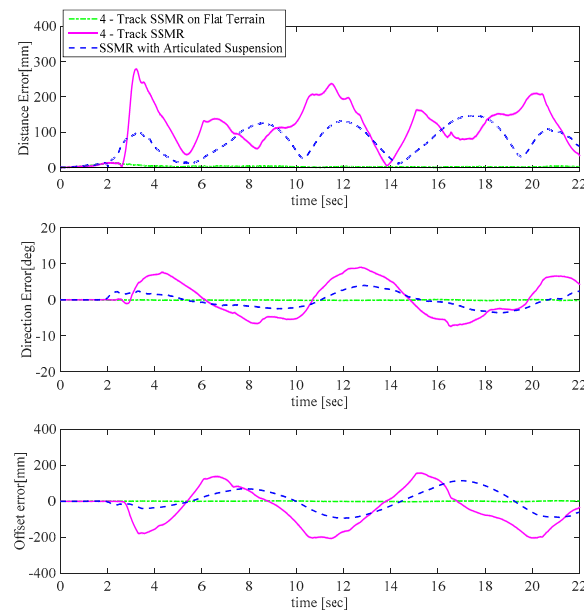


Figure 10. Comparison results of distance, direction, and offset errors of a non-suspension version of four track SSMR and PASTRo on flat and sinusoidal terrain: distance error, direction error, and offset error.

As shown in Table 5, the RMS distance, direction, and offset errors for PASTRo are 33.3, 56.3, and 43.2 percent smaller than the non-suspension version of the four-track MR, respectively. The proposed structural combination of a rocker and 2-DOF passive pitch-roll joints can improve posture tracking performance by maintaining a proper orientation in the driving tracks over rough terrain.

The distance, direction, and offset errors for PASTRo on the sinusoidal terrain are examined to compare the performance of the (1) TTCA-based driving velocity projection method and (2) velocity propagation-based driving velocity projection method. In addition, the three errors are also examined with conventional planar SSMR kinematics for comparison, as shown in Figure 11.

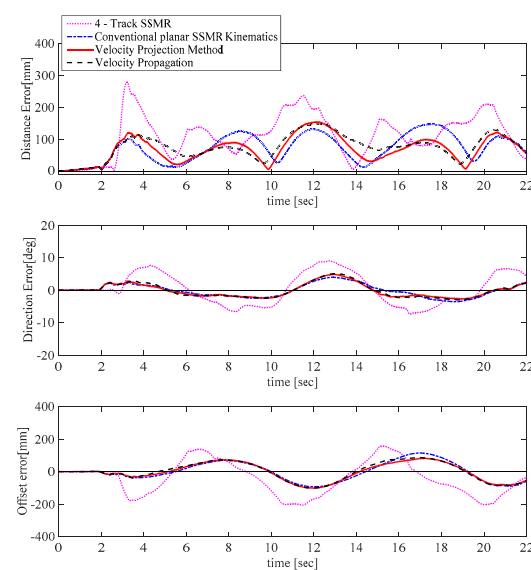


Figure 11. Comparison of maneuverability performances of the PASTRo in terms of the conventional SSMR kinematics, TTCA based driving velocity projection, and velocity propagation-based driving velocity projection methods on sinusoidal terrain: distance error, direction error, and offset error.

Table 6 shows that the RMS distance, direction, and offset errors of the TTCA driving velocity projection method are 8.8%, 3.8%, and 15.4%, smaller than those with conventional SSMR kinematics. The RMS distance, direction, and offset errors of the velocity propagation-based method are 3.31%, −3.33%, and 11.84% percent smaller than those with conventional SSMR kinematics, respectively. While the distance errors for both proposed methods in the downhill section are larger than those for conventional SSMR kinematics, the TTCA-based driving velocity projection-based method significantly improves the distance and offset errors.

1. No suspension + planar SSMR kinematics;
2. Suspension + planar SSMR kinematics;
3. Suspension + GEC w/o backward propagation;
4. Suspension + GEC w/backward propagation.

Table 6. Maneuverability performance value.

RSM Error	Four Track SSMR	PASTRo			
		Conventional Planar SSMR Kinematics	TTCA Based Driving Velocity Projection	Velocity Propagation Based Driving Velocity Projection	
Distance error [mm]	130.8	87.2 [** 33.3%]	79.5	[** 39.2%, * 8.8%]	
Direction error [deg]	4.8	2.1 [** 56.3%]	2.0	[** 57.9%, * 3.8%]	
Offset error [mm]	111.3	63.2 [** 43.2%]	53.5	[** 51.9%, * 15.4%]	

* Percentage differences of RMS errors compared with the conventional planar SSMR kinematics. ** Percentage differences of RMS errors compared with results of the four track SSMR.

In fact, both velocity projection-based methods generate driving velocities larger than the planar SSMR kinematics to compensate for the tilting effects of driving tracks, and larger driving velocities in downhill sections lead to significant slippage and poor performance in terms of the distance and offset errors. On the contrary, the larger driving velocities in uphill sections lead to improved performance in the distance and offset errors.

In the case of the RMS direction error, the geometrical concept of the TTCA is the angle between the axes in the heading directions, so any information to compensate for errors in the heading direction is not included in both velocity projection-based methods. As a result, both methods do not show a significant performance improvement compared to the RMS direction error, even though the velocity propagation-based method shows a poor RMS direction error relative to planar SSMR kinematics. That is, any significant improvements in the maneuverability performance of PASTRo cannot be obtained from additional consideration of the violation of the assumption in Equation (4) of Section 3.1.

5. Discussion and Conclusions

This study compares the posture tracking performance for four-track SSMR and PASTRo in terms of the distance, direction, and offset errors under the RecurDyn-Simulink co-simulation framework. The posture-tracking errors for PASTRo are much smaller than those of the non-suspension version of a four-track mobile. Table 6 shows that PASTRo achieves a 33.3% lower RMS distance error, 56.3% lower RMS directional error, and 43.2% lower RMS offset error than the four-track SSMR, even with planar SSMR kinematics. Thus, these results confirm that the proposed structural combination of the rocker and passive pitch-roll joints can improve the posture-tracking performance on rough terrain.

The TTCA is calculated from the suspension kinematics to improve the posture tracking performance of PASTRo without any further information on the rough terrain, and the obtained TTCA is used in both methods discussed in this study. The results indicate that PASTRo, with the TTCA-based driving velocity projection, achieves 39.2% lower RMS distance error, 57.9% lower RMS directional error, and 51.9% lower RMS offset error than the four-track SSMR. Additionally, PASTRo with velocity propagation-based driving velocity projection shows a 35.5% lower RMS distance error, 54.8% lower RMS directional

error, and 49.9% lower RMS offset error than four track SSMR. The velocity propagation is confirmed to compensate for differences in front and rear driving velocities without significantly improving performance over the first method. In the case of the RMS direction error, the improvements in the direction error are not a result of either method but are due to the suspension structure of PASTRo.

The simulation results indicate that the TTCA-based driving velocity projection method used in this study can improve the RMS distance, direction, and offset errors of the four-track MR with a passively articulated suspension. In particular, when tracking the reference trajectories on arbitrarily rough terrain with a high elevation gap, the contribution of the first method and PASTRo will continue to increase as the elevation gap increases.

Author Contributions: Conceptualization, D.L.; methodology, D.L.; software, H.J.; validation, H.J.; formal analysis, D.L.; data curation, H.J.; writing—original draft preparation, D.L.; writing—review and editing, D.L.; visualization, H.J.; supervision, D.L. All authors have read and agreed to the published version of the manuscript.

Funding: This research was supported by the Basic Science Research Program through the National Research Foundation of Korea (NRF) funded by the Ministry of Education (NRF-2022 R1F1A10747 04); Institute of Information & communications Technology Planning & Evaluation (IITP) grant funded by the Korea government (MSIT) (No. 2022-0-00218); the MSIT (Ministry of Science and ICT), Korea, under the Innovative Human Resource Development for Local Intellectualization support program (IITP-2022-RS-2022-00156360) supervised by the IITP (Institute for Information & communications Technology Planning & Evaluation); Korea Institute for Advancement of Technology (KIAT) grant funded by the Korea Government (MOTIE) (N000P0017033) and (N000P0017123).

Informed Consent Statement: Not applicable.

Data Availability Statement: Data sharing not applicable.

Conflicts of Interest: The authors declare no conflict of interest.

References

- Lindemann, R.; Reid, L.; Voorhees, C. Mobility Sub-System for the Exploration Technology Rover. 1999. Available online: <https://trs.jpl.nasa.gov/bitstream/handle/2014/17115/99-0537.pdf?sequence=1> (accessed on 8 January 2022).
- NASA, Mars Rover Curiosity. 2015. Available online: http://www.nasa.gov/mission_pages/msl/index.html/ (accessed on 15 June 2022).
- Lee, D.; Lee, S.; Ku, N.; Lim, C.; Lee, K.-Y.; Kim, T.-W.; Kim, J.; Kim, S.H. Development of a mobile robotic system for working in the double-hulled structure of a ship. *Robot. Comput. Integr. Manuf.* **2010**, *26*, 13–23. [CrossRef]
- Kim, H.; Kim, D.; Yang, H.; Lee, K.; Seo, K.; Chang, D.; Kim, J. Development of a wall-climbing robot using a tracked wheel mechanism. *J. Mech. Sci. Technol.* **2008**, *22*, 1490–1498. [CrossRef]
- Raibert, M.; Blankespoor, K.; Nelson, G.; Playter, R. Bigdog, the rough-terrain quadruped robot. *IFAC Proc. Vol.* **2008**, *41*, 10822–10825. [CrossRef]
- Ma, J.; Susca, S.; Bajracharya, M.; Matthies, L.; Malchano, M.; Wooden, D. Robust multi-sensor, day/night 6-DOF pose estimation for a dynamic legged vehicle in GPS-denied environments. In Proceedings of the 2012 IEEE International Conference on Robotics and Automation, Saint Paul, MN, USA, 14–18 May 2012; pp. 619–626.
- Yamauchi, B.M. PackBot: A versatile platform for military robotics. In Proceedings of the Unmanned Ground Vehicle Technology VI, Bellingham, WA, USA, 13–15 April 2004; pp. 228–237.
- Lee, W.; Kang, S.; Kim, M.; Park, M. ROBHAZ-DT3: Teleoperated mobile platform with passively adaptive double-track for hazardous environment applications. In Proceedings of the 2004 IEEE/RSJ International Conference on Intelligent Robots and Systems (IROS) (IEEE Cat. No. 04CH37566), Sendai, Japan, 28 September–2 October 2004; pp. 33–38.
- Zhang, D.; Gao, Z. Hybrid head mechanism of the groundhog-like mine rescue robot. *Robot. Comput.-Integr. Manuf.* **2011**, *27*, 460–470. [CrossRef]
- DARPA. DARPA Robotics Challenge Program: 2012 to 2015. Available online: <https://www.youtube.com/watch?v=mpsXQCHrAIM/> (accessed on 25 September 2015).
- DARPA. DARPA Robotics Challenge 2015 Finals. Available online: <https://www.youtube.com/watch?v=dv9Wm20UrcU/> (accessed on 6 October 2015).
- Siegwart, R.; Lamon, P.; Estier, T.; Lauria, M.; Piguët, R. Innovative design for wheeled locomotion in rough terrain. *Robot. Auton. Syst.* **2002**, *40*, 151–162. [CrossRef]
- Thueer, T.; Krebs, A.; Siegwart, R. Comprehensive locomotion performance evaluation of all-terrain robots. In Proceedings of the 2006 IEEE/RSJ International Conference on Intelligent Robots and Systems, Beijing, China, 9–15 October 2006; pp. 4260–4265.

14. Caracciolo, L.; De Luca, A.; Iannitti, S. Trajectory tracking control of a four-wheel differentially driven mobile robot. In Proceedings of the 1999 IEEE International Conference on Robotics and Automation (Cat. No. 99CH36288C), Detroit, MI, USA, 10–15 May 1999; pp. 2632–2638.
15. Kozłowski, K.; Pazderski, D. Modeling and control of a 4-wheel skid-steering mobile robot. *Int. J. Appl. Math. Comput. Sci.* **2004**, *14*, 477–496.
16. Shuang, G.; Cheung, N.C.; Cheng, K.E.; Lei, D.; Xiaozhong, L. Skid steering in 4-wheel-drive electric vehicle. In Proceedings of the 2007 7th International Conference on Power Electronics and Drive Systems, Bangkok, Thailand, 27–30 November 2007; pp. 1548–1553.
17. Tarokh, M.; McDermott, G.J. Kinematics modeling and analyses of articulated rovers. *IEEE Trans. Robot.* **2005**, *21*, 539–553. [[CrossRef](#)]
18. Kim, J.; Jeong, H.; Lee, D. Performance optimization of a passively articulated mobile robot by minimizing maximum required friction coefficient on rough terrain driving. *Mech. Mach. Theory* **2021**, *164*, 104368. [[CrossRef](#)]
19. Jeong, H.; Yu, J.; Lee, D. Track HM Design for Dynamic Analysis of 4-tracked Vehicle on Rough Terrain Using Recurd. *Trans. Korean Soc. Mech. Eng. A* **2021**, *45*, 275–283. [[CrossRef](#)]
20. Kanayama, Y.; Kimura, Y.; Miyazaki, F.; Noguchi, T. A stable tracking control method for an autonomous mobile robot. In Proceedings of the 1990 IEEE International Conference on Robotics and Automation, Cincinnati, OH, USA, 13–18 May 1990; pp. 384–389.
21. Apostolopoulos, D.S. *Analytical Configuration of Wheeled Robotic Locomotion*; Carnegie Mellon University: Pittsburgh, PA, USA, 2001.
22. Haji, T.; Kinugasa, T.; Yoshida, K.; Amano, H.; Osuka, K. Maneuverability of flexible mono-tread mobile track (FMT). In Proceedings of the 2009 ICCAS-SICE, Fukuoka, Japan, 18–21 August 2009; pp. 3427–3432.
23. Michaud, S.; Richter, L.; Thueer, T.; Gibbesch, A.; Huelsing, T.; Schmitz, N.; Weiss, S.; Krebs, A.; Patel, N.; Joudrier, L. Rover chassis evaluation and design optimisation using the RCET. In Proceedings of the ASTRA, 9th ESA Workshop on Advanced Space Technologies for Robotic and Automation, Noordwijk, The Netherlands, 28–30 November 2006.
24. Zhang, P.; Deng, Z.; Hu, M.; Gao, H. Mobility performance analysis of lunar rover based on terramechanics. In Proceedings of the 2008 IEEE/ASME International Conference on Advanced Intelligent Mechatronics, Xi'an, China, 2–5 July 2008; pp. 120–125.
25. Ding, L.; Gao, H.; Deng, Z.; Song, P.; Liu, R. Design of comprehensive high-fidelity/high-speed virtual simulation system for lunar rover. In Proceedings of the 2008 IEEE Conference on Robotics, Automation and Mechatronics, Chengdu, China, 21–24 September 2008; pp. 1118–1123.
26. Thueer, T.; Siegwart, R. Mobility evaluation of wheeled all-terrain robots. *Robot. Auton. Syst.* **2010**, *58*, 508–519. [[CrossRef](#)]
27. Deng, Z.; Fan, X.; Gao, H.; Ding, L. Influence analysis of terramechanics on conceptual design of manned lunar rover's locomotion system. In Proceedings of the 2011 International Conference on Electronic & Mechanical Engineering and Information Technology, Heilongjiang, China, 12–14 August 2011; pp. 645–648.
28. Gupta, A.K.; Gupta, V.K. Design and development of six-wheeled Multi-Terrain Robot. In Proceedings of the 2013 International Conference on Control, Automation, Robotics and Embedded Systems (CARE), Jabalpur, India, 16–18 December 2013; pp. 1–6.
29. Michaluk, N. *Design Methods for Cost-Effective Teams of Mobile Robots in Uncertain Terrain*; Massachusetts Institute of Technology: Cambridge, MA, USA, 2014.
30. Paez, L.; Melo, K. A preliminary review on metrics for modular snake robots locomotion. In Proceedings of the 4th Annual IEEE International Conference on Cyber Technology in Automation, Control and Intelligent, Hong Kong, China, 4–7 June 2014; pp. 539–545.

Disclaimer/Publisher's Note: The statements, opinions and data contained in all publications are solely those of the individual author(s) and contributor(s) and not of MDPI and/or the editor(s). MDPI and/or the editor(s) disclaim responsibility for any injury to people or property resulting from any ideas, methods, instructions or products referred to in the content.